THE COMPANY OF
Biologists

RESEARCH ARTICLE

Extracellular cleavage of E-cadherin promotes epithelial cell extrusion

Adam G. Grieve[1],[*],[‡] and Catherine Rabouille[1],[2],[‡]

ABSTRACT

Epithelial cell extrusion and subsequent apoptosis is a key mechanism to prevent the accumulation of excess cells. By contrast, when driven by oncogene expression, apical cell extrusion is followed by proliferation and represents an initial step of tumorigenesis. E-cadherin (E-cad), the main component of adherens junctions, has been shown to be essential for epithelial cell extrusion, but its mechanistic contribution remains unclear. Here, we provide clear evidence that cell extrusion can be driven by the cleavage of E-cad, both in a wild-type and an oncogenic environment. We first show that CDC42 activation in a single epithelial cell results in its efficient matrix metalloproteinase (MMP)-sensitive extrusion through MEK signalling activation and this is supported by E-cad cleavage. Second, using an engineered cleavable form of E-cad, we demonstrate that, by itself, truncation of extracellular E-cad at the plasma membrane promotes apical extrusion. We propose that extracellular cleavage of E-cad generates a rapid change in cell–cell adhesion that is sufficient to drive apical cell extrusion. Whereas in normal epithelia, extrusion is followed by apoptosis, when combined with active oncogenic signalling, it is coupled to cell proliferation.

KEY WORDS: E-cadherin, Extrusion, CDC42, TEV protease, MMP, MDCK, Adhesion

INTRODUCTION

Cell number within an epithelium must be tightly controlled, as there is limited space within the epithelial niche. Striking the right balance in terms of cell number is challenging. Epithelia selectively counteract the addition of new cells in order to relieve potential overcrowding and to prevent the accumulation of new cells. One of the mechanisms by which this is achieved is through apoptosis, whereby cells are stimulated to undergo programmed cell death that is followed by extrusion (Andrade and Rosenblatt, 2011; Kuipers et al., 2014; Lubkov and Bar-Sagi, 2014).

Alternatively, live cells are removed from epithelia through the processes of apical extrusion or delamination (Denning et al., 2012; Eisenhoffer et al., 2012; Marinari et al., 2012). Importantly, these events are followed by apoptosis. Therefore, live-cell

[1]Hubrecht Institute-KNAW & University Medical Center Utrecht, Uppsalalaan 8, 3584 CT Utrecht, The Netherlands. [2]The Department of Cell Biology, UMC Utrecht, The Netherlands.
*Present address: Sir William Dunn School of Pathology, University of Oxford, South Parks Road, Oxford OX1 3RE, UK.

[‡]Authors for correspondence (c.rabouille@hubrecht.eu; adam.grieve@path.ox.ac.uk)

extrusion and subsequent apoptosis has been proposed to be a tumour-suppressive process that prevents the formation of multi-layered epithelia (Eisenhoffer et al., 2012; Eisenhoffer and Rosenblatt, 2013).

Events of live-cell extrusion have also been observed upon the activation of different oncogenes (such as K-Ras, H-Ras, Src and ERBB2) within single cells of an epithelium (Hogan et al., 2009; Kajita et al., 2010; Leung and Brugge, 2012; Slattum et al., 2014; Wu et al., 2014). These oncogene-driven extrusion events are subsequently coupled to proliferation, not apoptosis. Saliently, extrusion is rate limiting to proliferation, indicating that cells must first escape a growth-suppressive environment within the epithelium in order to proliferate (Leung and Brugge, 2012). As transformation occurs in a single cell surrounded by histologically normal epithelial tissue (Nowell, 1976), oncogene-driven apical cell extrusion is considered to be a model for the initial stages of tumorigenesis.

The molecular mechanisms that govern live-cell extrusion are not well understood, although a few key components are emerging. A general requirement for Rho kinase (ROCK) activity both in wild-type and H-Ras-mediated extrusion suggests that actomyosin dynamics are crucial to live-cell extrusion (Hogan et al., 2009; Eisenhoffer et al., 2012). Furthermore, activity of the small Rho GTPase CDC42 has also been shown to be required for H-Ras-mediated apical cell extrusion (Hogan et al., 2009). Like ROCK, CDC42 has key roles in actin remodelling (Tapon and Hall, 1997); however, it also has trafficking functions (Harris and Tepass, 2010) as well as signalling roles, most notably contributing to the MEK–ERK signalling cascade (Coso et al., 1995; Minden et al., 1995). Interestingly, activation of ERBB2, H-Ras and Src leads to upregulated ERK signalling, and ERK inhibition blocks apical extrusion (Hogan et al., 2009; Kajita et al., 2010; Leung and Brugge, 2012). ERK signalling can drive the transcriptional upregulation of matrix metalloproteinase (MMP) family members (Lincoln and Bove, 2005). This observation is particularly interesting given that ERBB2-transformed cells require MMP activity to apically translocate (Leung and Brugge, 2012). However, the substrate(s) of MMP activities in this context are unknown.

Lastly, cell–cell adhesion, in particular E-cadherin (E-cad)-mediated adhesion, significantly contributes to apoptotic and non-apoptotic extrusion in vitro and in vivo (Hogan et al., 2009; Denning et al., 2012; Leung and Brugge, 2012; Lubkov and Bar-Sagi, 2014). E-cad is a key component of adherens junctions (Riethmacher et al., 1995; Gumbiner, 2000; Gottardi et al., 2001), which are linked to the underlying cytoskeleton through binding of the E-cad cytoplasmic domain to catenins (Gumbiner, 2000; Baum and Georgiou, 2011; Desai et al., 2013). As a result, trans-dimerisation of E-cad links cells together and stimulates actin polymerisation (Gumbiner, 2000; Patel et al., 2003). Accordingly,

E-cad is essential to epithelial polarisation (Capaldo and Macara, 2007).

Interestingly, depletion of E-cad from the epithelia surrounding an active H-Ras-expressing cell specifically blocks apical cell extrusion (Hogan et al., 2009), highlighting an interesting yet not well understood interplay between an extruding cell and its neighbours. Loss of E-cad expression in whole monolayers leads to defects in apoptotic extrusion (Lubkov and Bar-Sagi, 2014) and, likewise, p120-catenin depletion in the whole epithelium blocks the apical cell translocation of ERBB2-positive cells (Leung and Brugge, 2012). Despite these observations, the exact contribution of E-cad to apical cell extrusion is not known and, more generally, the initial series of events that trigger cell extrusion is unclear.

As mentioned above, MMP activity contributes to oncogene-driven apical cell extrusion (Leung and Brugge, 2012). Furthermore, E-cad can be cleaved by MMPs at sites within its extracellular domains, resulting in a loss of its adhesive properties (Marambaud et al., 2002; Maretzky et al., 2005). This led us to hypothesise that extracellular cleavage of E-cad endows cells with the potential to extrude, especially if E-cad cleavage is concentrated at the interface between one epithelial cell and its neighbours.

Here, we show that Madin-Darby canine kidney (MDCK) cells expressing active CDC42 are efficiently extruded in an ERK-signalling-dependent manner and that extrusion is supported by MMP-mediated E-cad cleavage. To directly test our hypothesis, we generated a form of E-cad that could be cleaved by tobacco etch virus protease (TEVp), and we show that extracellular truncation of E-cad at the plasma membrane of one epithelial cell is sufficient to drive its apical cell extrusion.

RESULTS
Constitutively active CDC42 drives epithelial extrusion

Cell extrusion has been observed in single cells expressing oncogenic H-Ras (H-RasV12) surrounded by wild-type cells (Hogan et al., 2009), and this event requires ROCK and CDC42 activity. Because co-transfection with dominant-negative CDC42 (CDC42N17) is known to block this extrusion (Hogan et al., 2009), we tested whether increased CDC42 activity alone is sufficient to specifically drive apical cell extrusion. To test this, we assessed the extrusion potential of single MDCK cells expressing a constitutively active form of CDC42 (GFP–CDC42V12) in what we term a heterologous cell system (i.e. in the context of a wild-type epithelium). As early as 8 h post-transfection, we observed a high rate of extrusion of CDC42V12 cells ($93\pm1.4\%$; $\pm$s.e.m.) compared with that of control GFP-expressing cells ($8.6\pm1.3\%$) (Fig. 1A,B), and we also observed a lack of extrusion with wild-type CDC42 or CDC42N17 (supplementary material Fig. S1A). GFP–HRasV12-expressing cells were also extruded but only after 24 h and at lower efficiency ($40\pm2.6\%$, Fig. 1C, right panel). As with H-Ras-mediated transformation, cells expressing GFP–CDC42V12 form multilayered colonies that remain attached to the underlying epithelial monolayer after 24 h, with $87\pm3.4\%$ of GFP–CDC42V12 cells above the monolayer in large adherent clumps (Fig. 1C, left panel). Importantly, 90% of single cells extrude at 8 h, demonstrating that extrusion does not require the concerted actions of a group of proliferating cells.

We next asked whether actomyosin dynamics within the CDC42V12-expressing extruding cell has a role in its extrusion.

To investigate this, we co-transfected cells with dominant-negative versions of the Rho GTPases Rac1(N17) or RhoA(N19), along with GFP–CDC42V12. Our analyses revealed no significant change in CDC42V12-driven cell extrusion (supplementary material Fig. S1B,C), suggesting that the actomyosin dynamics previously shown to be required for extrusion (Hogan et al., 2009; Kajita et al., 2010; Leung and Brugge, 2012) are not a major contributor within the extruded cell itself.

To test whether CDC42V12-mediated apical cell extrusion, like that shown for H-RasV12 (Hogan et al., 2009), is driven by downstream MEK signalling as suggested previously (Fanger et al., 1997), we used the MEK inhibitor U0126 and found a significant block in extrusion (Fig. 1B,D,D′). Treatment with U0126 coincided with the loss of the rosette-like basal actin accumulation frequently observed during extrusion (Fig. 1D′). The inhibition of extrusion with UO126 demonstrates that the role for CDC42 is mediated by downstream MEK signalling and is seemingly independent of the direct roles played by CDC42 in actin polymerisation and E-cad endocytosis (Georgiou et al., 2008; Leibfried et al., 2008; Shen et al., 2008).

E-cad is extracellularly cleaved in CDC42V12-transfected cells

E-cad-mediated adhesion plays a key role in the apical extrusion of cells expressing oncogenes (Hogan et al., 2009; Wu et al., 2014). Accordingly, under low-Ca^{2+} growth conditions (leading to loss of E-cad adhesion), CDC42V12-driven single-cell extrusion was blocked (supplementary material Fig. S1D). Collectively, these data led us to examine whether E-cad is modified upon transfection of CDC42V12.

We first monitored endogenous E-cad in GFP–CDC42V12-transfected epithelia by immunofluorescence, using an antibody that recognised the extracellular domain (anti-E-cadEC, see Fig. 2A). In GFP–CDC42V12-expressing extruding cells, the level of E-cad appeared to be reduced when compared with that of GFP-expressing cells (Fig. 2B′,C′, arrows), whereas the actin-labelling intensity was increased (Fig. 2B′, arrowhead). We observed that, during extrusion, surrounding cells create a new adherens junction underneath the extruding cell (Fig. 2B′,C′, double arrows). This presumably functions to seal the gap left by extruded GFP–CDC42V12 cells, akin to that recently shown during apoptotic cell extrusion (Lubkov and Bar-Sagi, 2014).

We performed quantitative line-scan analysis of the E-cad labelling intensity at the plasma membrane in the extruded portion of the cell (Fig. 2D, '3'). This was reduced to ~20% of the level measured at the control GFP-transfected cell interface with wild-type cells (Fig. 2D, '1' $n=<20$), with a 20% increase in actin label. This decrease could either be part of the mechanism that drives cell extrusion or a consequence of it. Therefore, we measured the E-cad level at the remaining interface between a CDC42V12-expressing extruding cell and its wild-type neighbours (Fig. 2D, '2'). This revealed a ~50% decrease compared with that of control GFP-transfected cell interfaces with wild-type cells (Fig. 2D, '1'), suggesting that the decrease in E-cad precedes extrusion.

We further investigated this apparent loss of E-cad upon transfection with GFP–CDC42V12. Western blots of cell lysates revealed a significant increase in the intensity of a 35-kDa band (2.3 ± 0.2-fold, $n=3$, $\pm$s.e.m.) detected by an antibody recognising the E-cad cytoplasmic domain (anti-E-cadCD, see Fig. 2A), suggesting that full-length E-cad is cleaved (Fig. 3A).
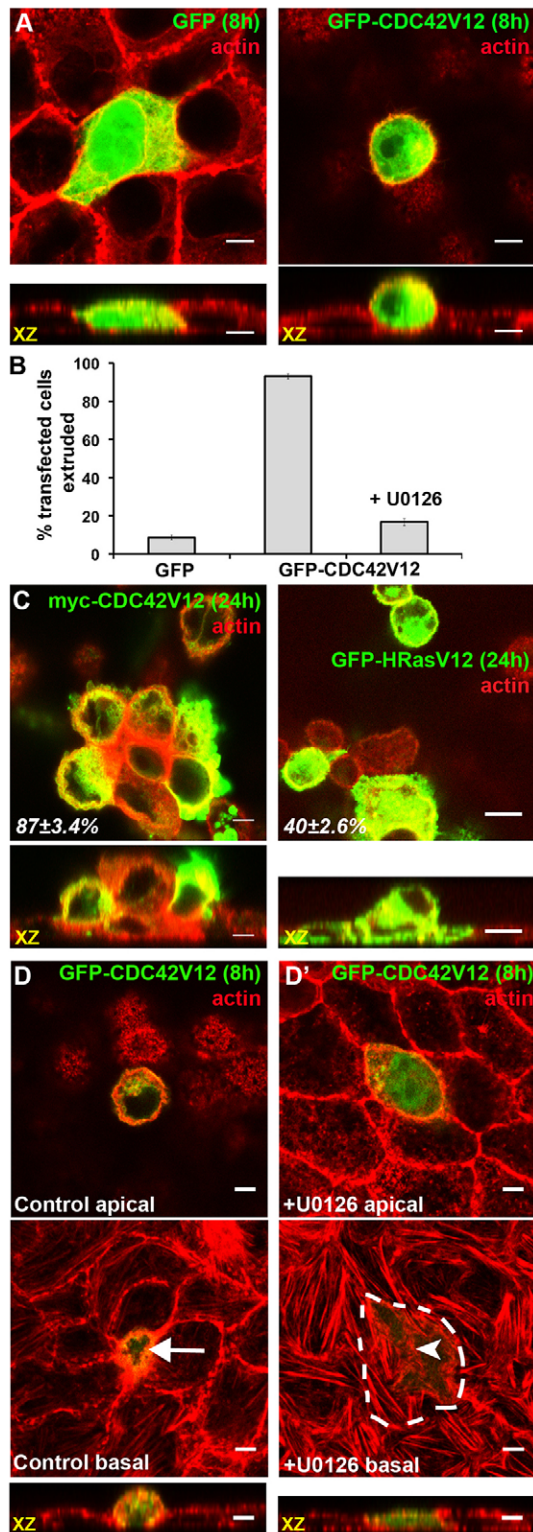
Fig. 1. Constitutively active CDC42 drives epithelial extrusion.
(A) Visualisation by fluorescence microscopy of actin (phalloidin, red) and GFP (green) in MDCK cells transfected with GFP and GFP–CDC42V12 for 8 h. An XZ (orthogonal) view displays cell extrusion as defined in Materials and Methods. (B) Quantification of the extrusion of cells transfected for 8 h with GFP (70 cells) or GFP–CDC42V12 (129 cells) that were either untreated or incubated for 6 h with U0126 (54 cells). 100% represents the extrusion of all transfected cells. Data show the mean±s.e.m. (n=3). (C) Visualisation by (immuno)fluorescence microscopy of actin (phalloidin, red) and Myc–CDC42V12 (green) or GFP–HRasV12 (green) in cells transfected for 24 h (n=3). (D,D′) Visualisation of apical and basal fluorescence of actin (phalloidin, red) and GFP (green) in cells transfected with GFP–CDC42V12 for 8 h that were either mock treated (D) or incubated with U0126 (D′). Note that, after U0126 treatment, the strong accumulation of actin underneath GFP–CDC42V12 transfected cells (arrow) is lost (arrowhead). The white dashed line corresponds to the plasma membrane of the transfected cell. Scale bars: 5 μm [A, C (left panel), D], 10 μm (C, right panel).

35-kDa band (2.5±0.6-fold, n=4), leading us to propose that upon CDC42 activation the extracellular domain of E-cad is cleaved (Fig. 3B). We questioned whether E-cad cleavage was also evident upon transfection with GFP–HRasV12, which also drives cell extrusion (Hogan et al., 2009; Fig. 1C, right). Indeed, we found that GFP–HRasV12 transfection led to an increase in cleaved E-cad at the plasma membrane (supplementary material Fig. S1E).

Activation of MEK signalling is required for extrusion and E-cad cleavage of CDC42V12-transfected cells

We have demonstrated that the MEK inhibitor U0126 efficiently blocks CDC42V12-mediated cell extrusion (Fig. 1B,D,D′). If E-cad cleavage promotes the process of CDC42V12-driven cell extrusion, U0126 treatment should lead to a relative decrease in the 35-kDa E-cad cleavage product. By western blot analysis, U0126 was found to strongly block E-cad cleavage, and E-cad cleavage positively correlated with CDC42V12-driven cell extrusion (Fig. 3C). To confirm the involvement of the MEK pathway, we showed that the overexpression of a constitutively active form of MEK1 (MEK1DD) stimulated apical cell extrusion (Fig. 3D–D″, 61.5±1.2%, ±s.e.m.), in line with previous reports (Leung and Brugge, 2012). As expected, overexpression of active MEK1 also led to an increase in E-cad cleavage (3.9±0.3-fold) compared with that of control GFP transfections (Fig. 3E), further demonstrating the positive correlation between E-cad cleavage and epithelial extrusion.

Extracellular cleavage of E-cad in CDC42V12-transfected cells is driven by MMP activity and promotes extrusion

We tested whether MMPs are involved in CDC42V12-mediated E-cad cleavage, as shown for ERBB2-driven extrusion (Leung and Brugge, 2012). Treatment with the broad MMP inhibitor GM6001 led to a significant decrease (58±7%, n=3, ±s.e.m.) in the levels of the 35-kDa E-cad cleavage fragment at the plasma membrane in GFP–CDC42V12-transfected cells (Fig. 4A, compare lanes 2 and 4). Similar effects were obtained with another MMP inhibitor, batimastat (data not shown). Strikingly, the observed loss of E-cad cleavage upon treatment with GM6001 or batimastat is accompanied by a 60–70% reduction in CDC42V12-mediated extrusion (Fig. 4B,C).

As CDC42V12-mediated extrusion was inhibited by the MEK inhibitor U0126, we hypothesised that ERK signalling leads to the transcriptional upregulation of a specific protease. Therefore, we performed an RT-qPCR screen, focused on 13 candidate proteases. We found that active CDC42 signalling led to the

The molecular mass of this fragment indicates that it corresponds to an E-cad cleavage product encompassing the cytoplasmic and transmembrane domain (Fig. 2A).

To test whether this cleaved product is present at the plasma membrane, we biotinylated plasma membrane proteins and performed streptavidin pull-downs, followed by western blotting. This recapitulated the increase in the intensity of the
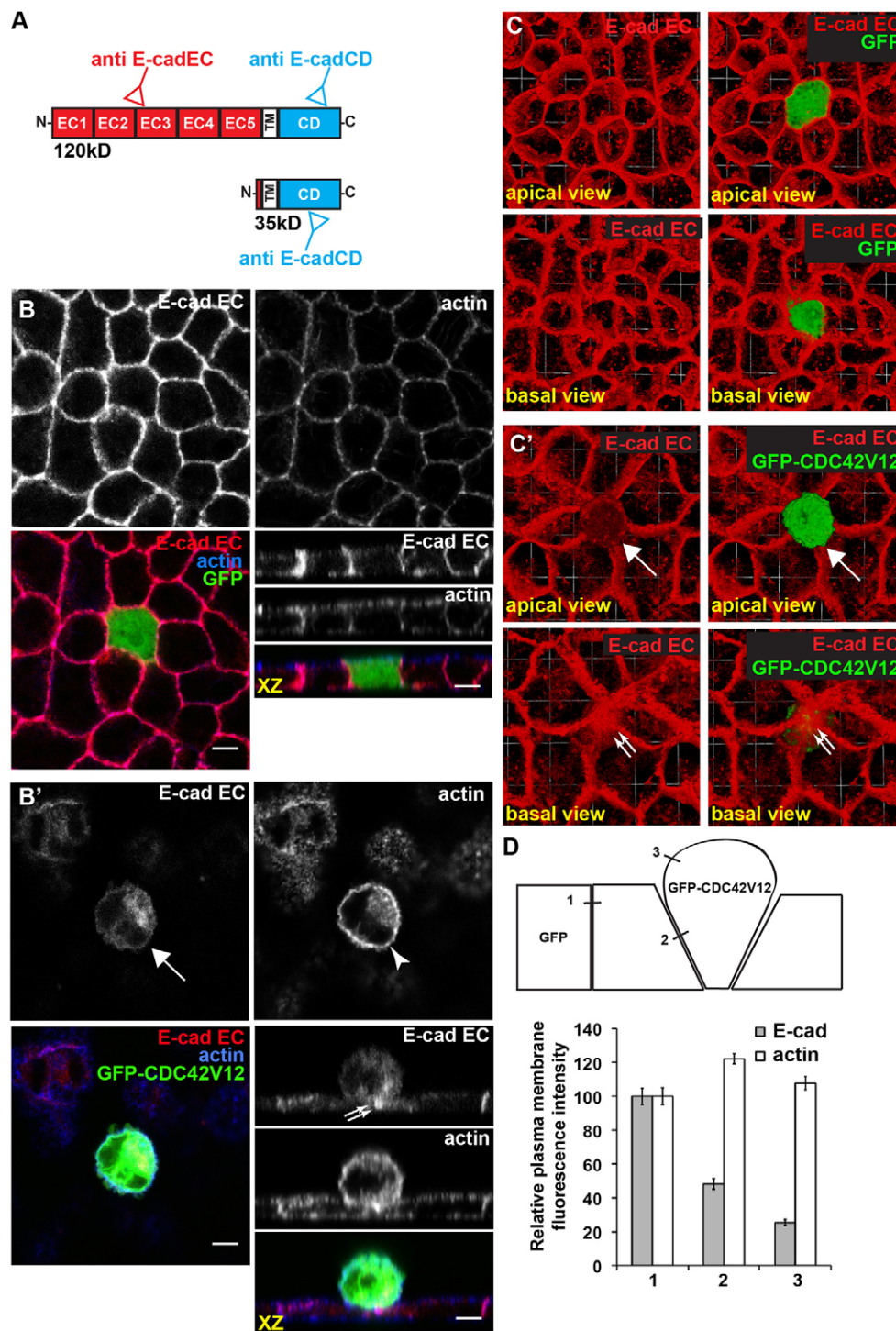
Fig. 2. The amount of plasma-membrane-associated E-cad is reduced in CDC42V12 extruding cells. (A) Schematic of E-cad domain structure. The anti-E-cadEC antibody (red) recognises the extracellular domains (EC1–5) of E-cad, thus detecting full-length 120-kDa E-cad. The anti-E-cadCD antibody (blue) recognises the E-cad cytoplasmic domain (CD), so both full-length (120 kDa) and cleaved E-cad (35 kDa) are recognised. (B,B′) Visualisation by fluorescence microscopy of E-cad using anti-E-cadEC (red) and actin (phalloidin, blue) in MDCK cells transfected with GFP (B) or GFP–CDC42V12 (B′) for 8 h. The XZ view also is displayed. (C,C′) Three-dimensional projections of apical or basal views (using Volocity 3D Image Analysis, Perkin Elmer) of the localisation of E-cad (anti-E-cadEC, red) in cells transfected with GFP (D) or GFP–CDC42V12 (D′) (green) for 8 h. Arrows indicate transfected cells with reduced E-cad; the arrowhead indicates increased levels of actin; double arrows indicate the accumulation of E-cad underneath extruding cells. (D) Quantification of E-cad and actin fluorescence intensities at three plasma membrane domains (1–3, depicted in the diagram) in GFP- and GFP–CDC42V12-expressing cells. Data show the mean±s.e.m. (GFP, $n=14$ cells; GFP–CDC42V12, $n=20$ cells). Scale bars: 5 μm.
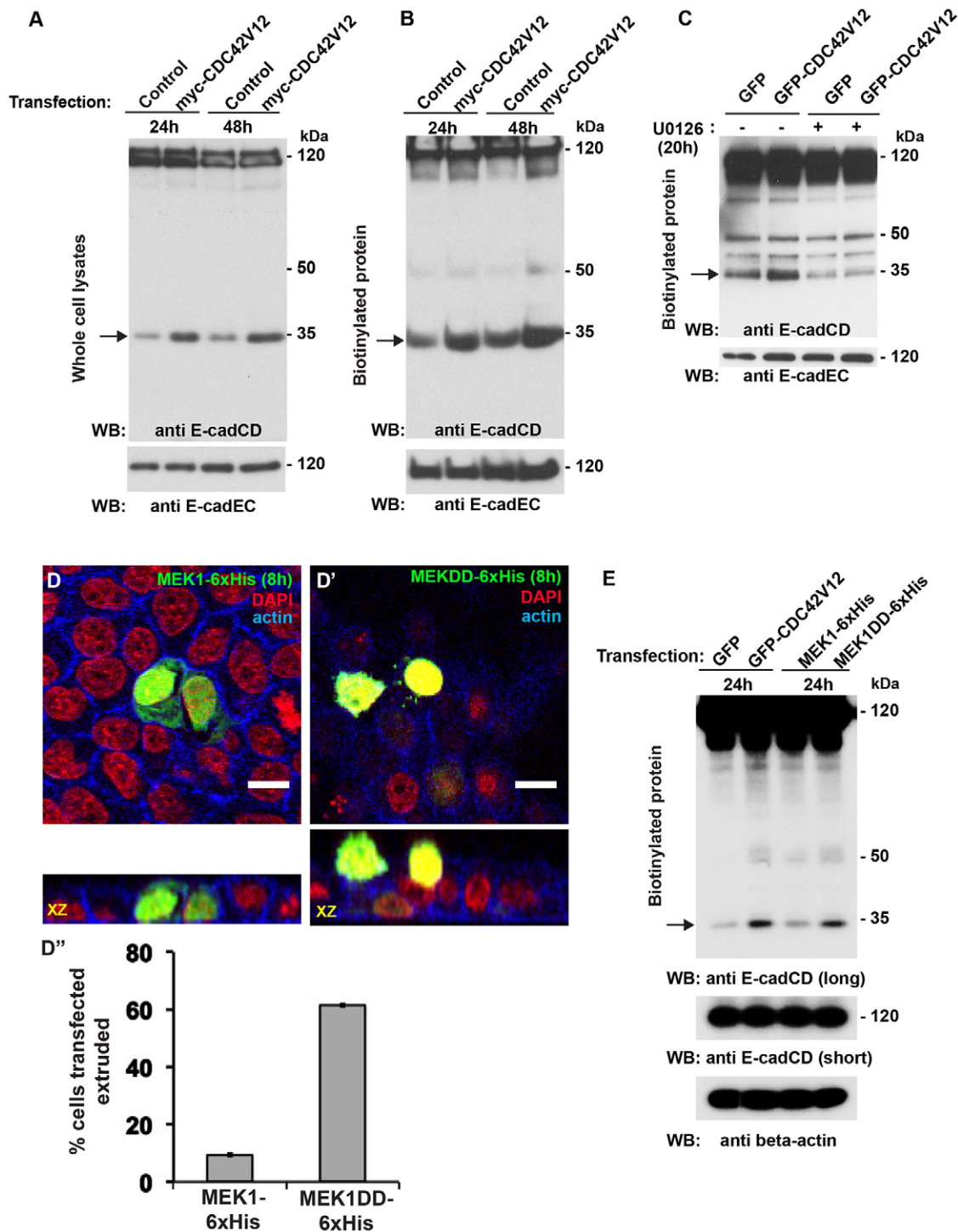
Fig. 3. Activation of CDC42 leads to enhanced E-cad cleavage through activation of the MEK pathway. (A) Western blot (WB) of lysates of MDCK cells transiently expressing empty vector (control) or Myc–CDC42V12 for 24 or 48 h using antibodies against E-cadCD or E-cadEC (see Fig. 2A). (B) Western blot of biotinylated plasma membrane proteins of cells transiently transfected with empty vector (control) or Myc–CDC42V12 for 24 or 48 h using antibodies against E-cadCD or E-cadEC. (C) Western blot of biotinylated plasma membrane proteins of cells transiently transfected with GFP (control) or GFP–CDC42V12 for 24 h, incubated with or without the MEK inhibitor U0126 for 20 h, using antibodies against E-cadCD or E-cadEC. (D,D′) Representative (immuno)fluorescence images of cells transfected with MEK1–6×His (D) or MEK1DD–6×His (D′) for 8 h (anti-6×His, green), also showing nuclei (DAPI, red) and actin (phalloidin, blue). Scale bars: 10 µm. (D″) Quantification of the extrusion of MDCK cells transfected with MEK1–6×His (n=66 cells) or MEK1DD–6×His (n=75 cells) for 8 h. Data show the mean±s.e.m. (n=3). (E) Western blot of biotinylated plasma membrane proteins from cells transiently transfected with GFP (control), GFP–CDC42V12, MEK1–6×His or MEK1DD–6×His for 24 h using anti-E-cadCD, along with blotting of the cellular inputs. β-actin served as a loading control. Exposure length (long, short) is indicated. Arrows indicate the 35-KDa E-cad cleavage product.
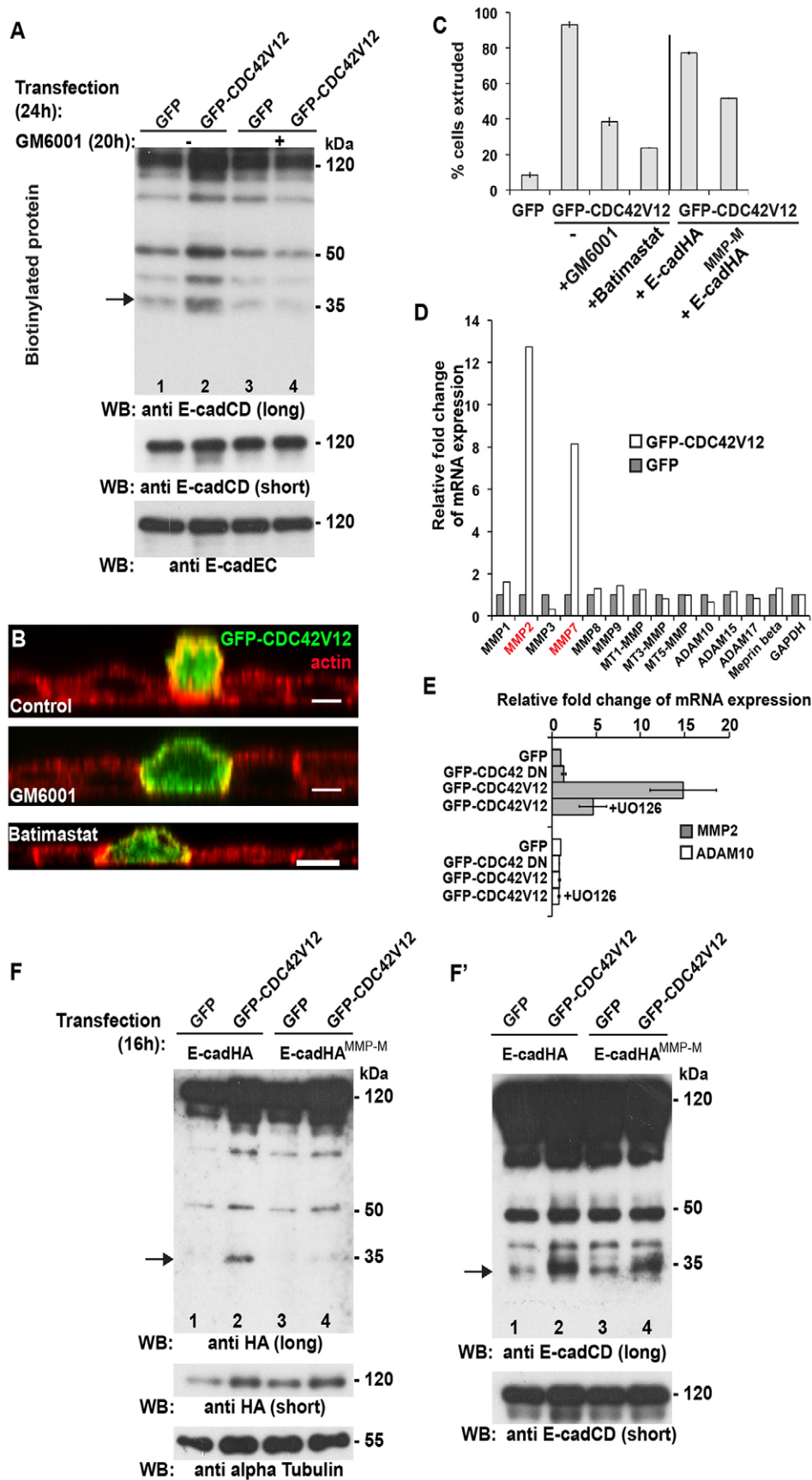
Fig. 4. See next page for legend.

Fig. 4. CDC42-mediated E-cad cleavage and cell extrusion is MMP dependent. (A) Western blot (WB) of biotinylated plasma membrane proteins from transiently transfected MDCK cells expressing GFP or GFP–CDC42V12 (24 h) that were incubated with or without GM6001 for 20 h. Blotting was performed using antibodies against E-cadCD and E-cadEC. (B) XZ fluorescence images showing actin (phalloidin, red) and GFP (green) in cells transfected with GFP–CDC42V12 in DMSO (control) or in the presence of the MMP inhibitors GM6001 or batimastat. Scale bars: 5 μm. (C) Quantification of the extrusion of cells transfected for 8 h with GFP ($n=70$ cells) or GFP–CDC42V12 ($n=129$ cells), then untreated or incubated for 6 h with the MMP inhibitors GM6001 ($n=91$ cells) or batimastat ($n=76$ cells). Extrusion was also quantified for cells that were transfected with E-cadHA ($n=149$ cells) or a form of E-cadHA with a mutated MMP cleavage site (E-cadHA[MMP-M], see Fig. 5A and Fig. 3F) ($n=155$ cells). 100% represents extrusion of all transfected cells. Data show the mean±s.e.m. ($n=3$). (D) The fold change in mRNA expression level (as determined by using RT-qPCR) of 13 proteases upon transfection with GFP or GFP–CDC42V12 for 24 h, relative to the control, GAPDH. Data show the mean. (E) The effect of U0126 treatment (for 20 h) on the upregulation of MMP2 in cells transfected with GFP–CDC42V12 (24 h) was measured by RT-qPCR. Expression is shown relative to that of the control, GAPDH. Data show the mean±s.e.m. (F,F′) Western blots of biotinylated membrane preparations from MDCK cells that transiently expressed GFP, GFP–CDC42V12, E-cadHA or E-cadHA[MMP-M] for 16 h (see C), using antibodies against HA (F) or E-cadCD (F′). The transfection efficiency is ~20%. Exposure length (long, short) is indicated. Arrows indicate the 35-kDa E-cad cleavage product.

specific upregulation of MMP2 and MMP7 mRNAs (a representative dataset is shown in Fig. 4D), in an U0126-sensitive manner, at least for MMP2 (Fig. 4E).

To conclusively confirm that the observed 35-kDa fragment in CDC42V12-transfected cells is due to MMP activity, we mutated the predicted MMP site in E-cad (Marambaud et al., 2002) (Fig. 5A). We transiently co-transfected this mutant form of E-cad (E-cadHA[MMP-M]) along with GFP–CDC42V12 for 16 h and performed plasma membrane biotinylation assays. The 35-kDa E-cadHA fragment generated in response to transfection with GFP–CDC42V12 (Fig. 4F, lane 2) is not observed with E-cadHA[MMP-M] (Fig. 4F, compare lanes 2 and 4), thus further confirming that E-cad is cleaved by MMPs upon activation of CDC42.

We then tested whether transfection of E-cadHA[MMP-M] had an inhibitory effect on GFP–CDC42V12-driven extrusion. When compared with co-transfection of E-cadHA, GFP–CDC42V12-transfected cells were extruded ~33% less efficiently when co-transfected with E-cadHA[MMP-M] (Fig. 4C). This represents a strong effect on CDC42V12-mediated extrusion, especially considering that a significant pool of endogenous E-cad is cleaved in this context (Fig. 4F′, compare lanes 2 and 4). Taken together, these results suggest that signalling elicited by activated CDC42 upregulates MMP activity that catalyses extracellular cleavage of E-cad at the plasma membrane, which promotes apical cell extrusion.

Engineering a TEVp-cleavable form of E-cad, Cle-cadHA

Collectively, these data suggest that a change in the adhesive property of one cell is sensed by wild-type epithelia and can trigger epithelial cell extrusion. We therefore hypothesise that, on its own, extracellular cleavage of E-cad at the plasma membrane of one cell within an epithelium causes a rapid change in cell–cell adhesion that is sufficient to promote cell extrusion.

To test whether E-cad cleavage at the plasma membrane is sufficient to promote cell extrusion, we engineered a cleavable form of E-cad (termed Cle-cad). Cle-cad is identical to E-cad except for the insertion of a TEVp cleavage site (amino acid sequence ENLYFQG) between the E-cad transmembrane domain

and its adjacent extracellular domain (EC5). As the major adhesive property of E-cad resides within EC1 (and EC2 to a lesser extent) (Chitaev and Troyanovsky, 1998; Patel et al., 2003) (Fig. 5A), TEVp-mediated cleavage should eliminate its adhesive properties.

Cle-cadHA displayed the same localisation to adherens junctions as E-cadHA (as well as a faint Golgi localisation), and the expression of these proteins did not alter cell morphology, polarisation or survival (Fig. 5B; supplementary material Fig. S2A). Furthermore, using a buffer previously shown to extract labile protein from cells and preserve the actin cytoskeleton (CSK buffer), we found that Cle-cadHA was incorporated into adherens junctions marked by residual actin label as efficiently as E-cadHA (supplementary material Fig. S2B). Moreover, this insertion yielded a specific cleavable form of E-cad. The addition of TEVp to immunoprecipitated Cle-cadHA in vitro resulted in the specific and expected loss of full-length Cle-cad at 120 kDa ($58\pm5\%$ reduction, $n=4$, ±s.e.m.) (Fig. 5C), as observed by western blotting using either anti-E-cadEC (lanes 3–4) or anti-E-cadCD (lanes 1–2). It also led to the concomitant production of a cleaved product at 35 kDa (7.6 ± 0.9-fold increase, $n=4$) corresponding to the E-cad cytoplasmic and transmembrane domain (therefore recognised only by anti-E-cadCD) (Fig. 5C; lanes 1–2).

To test TEVp activity in vivo, we generated E-cadHA- and Cle-cadHA-expressing stable cell lines that were grown on permeable Transwell filters, thus enabling the addition of TEVp to the basal medium and accessibility of the protease to adherens junctions. The addition of TEVp to the basal medium for 3 h had no effect on E-cadHA levels when assessed by western blotting (1.2 ± 0.1-fold compared with control, $n=3$) (Fig. 5D, compare lanes 1 and 2). By contrast, we observed a rapid loss of Cle-cadHA ($84\pm3\%$ reduction in the intensity of the 120-kDa band compared with the control, $n=3$) (Fig. 5D, compare lanes 3 and 4). Accordingly, plasma-membrane-associated Cle-cadHA immunofluorescence was specifically lost upon treatment with TEVp (Fig. 5F, first row; Fig. 5G). Taken together, these results show that, in vivo and in vitro, TEVp can efficiently cleave Cle-cadHA.

Unlike the in vitro cleavage (Fig. 5C, lane 2), the concomitant accumulation of the cleaved 35-kDa fragment after TEVp treatment in vivo was not observed (Fig. 5D; lane 4). Timecourse studies revealed that the majority of Cle-cadHA was depleted within 1 h of TEVp addition, and the cleaved 35-kDa product was faintly detected within this timeframe before disappearing, suggesting that it is rapidly degraded (supplementary material Fig. S2C). Incubation with the proteasomal inhibitor MG132 during TEVp cleavage (but not with the lysosomal inhibitor bafilomycin A) led to the accumulation of this fragment (13.5 ± 2.7-fold increase compared with the control, $n=3$) (supplementary material Fig. S2D; compare lanes 4–6). This suggests that, during short periods of extracellular cleavage, cleaved E-cad is recognised and degraded by the cytoplasmic proteasomal machinery, as shown previously (Fujita et al., 2002; Hartsock and Nelson, 2012). Importantly, regardless of the degradative fate of truncated E-cad, the addition of TEVp led to efficient plasma membrane cleavage of full-length Cle-cad.

We next asked how much Cle-cadHA is expressed relative to the total level of E-cad within our stable cell line. To address this, we performed immunoprecipitations of total E-cad using anti-E-cadCD. Upon subsequent treatment with TEVp in vitro, we showed using an anti-HA antibody that, as expected, Cle-cadHA was efficiently cleaved (supplementary material Fig. S2E, lanes 1
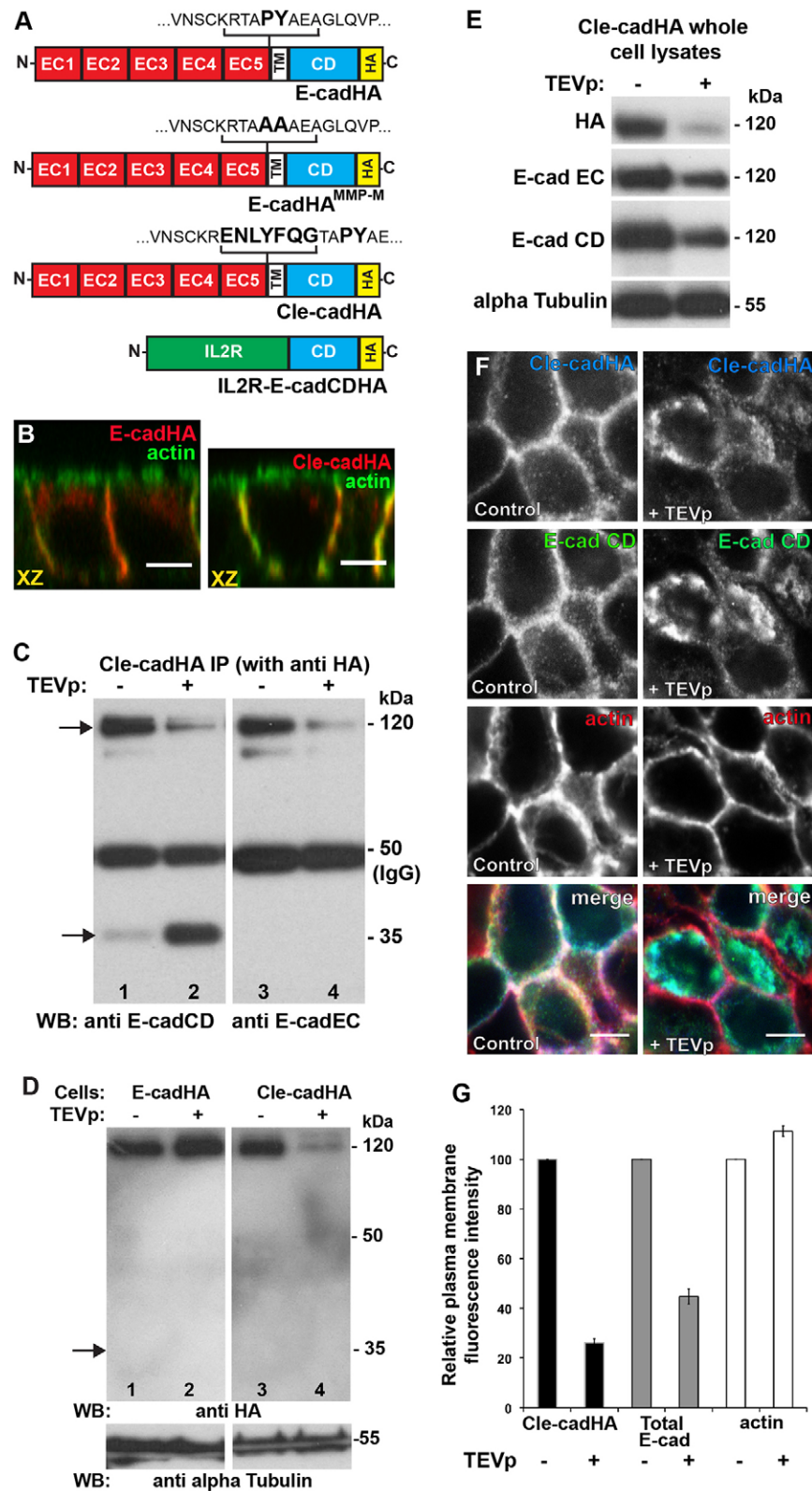
Fig. 5. See next page for legend.

and 2). In parallel, using anti-E-cadEC, we observed a $38.1\pm6.3\%$ reduction in total E-cad (supplementary material Fig. S2E, lanes 3 and 4). This suggests that a significant proportion of total E-cad is replaced by Cle-cadHA. This result

was reproduced *in vivo*. Western blot analysis showed that after 3 h of TEVp treatment of Cle-cadHA-expressing cells, the total level of E-cad, as determined using anti-E-cadEC and anti-E-cadCD antibodies, was reduced by $41.5\pm2.4\%$ (Fig. 5E).

Fig. 5. Engineering and characterisation of a TEVp-cleavable form of E-cad, Cle-cadHA. (A) Schematic representation of the forms of HA-tagged E-cad used in this study. In E-cadHA, the five extracellular domains (EC1–5) are represented in red, the transmembrane (TM) domain in white, cytoplasmic domain in blue and HA tag in yellow. The PY residues, shown in bold, are the predicted amino acid residues of the MMP cleavage site. PY residues are mutated to AA in E-cadHA^{MMP-M}. Cle-cadHA differs from E-cad by the insertion of the TEVp cleavage site (ENLYFQG, in bold) between the transmembrane domain and EC5, upstream of the intact MMP site. IL2R–E-cadCDHA comprises the cytoplasmic domain of E-cad linked to the transmembrane and extracellular domain of IL2R (green).
(B) (Immuno)fluorescence images showing actin (phalloidin, green) and HA (red) in MDCK cells stably expressing either E-cadHA or Cle-cadHA and cultured on Transwell filters. An XZ (orthogonal) view demonstrates identical cell polarity and subcellular localisation. (C) Western blot (WB) of immunoprecipitated Cle-cadHA (using antibody against HA) that was incubated for 3 h *in vitro* with or without purified TEVp. Blotting was performed using antibodies against E-cadCD or E-cadEC. (D) Western blot of lysates from MDCK cells stably expressing E-cadHA or Cle-cadHA, grown on Transwell filters and incubated for 3 h with (+) or without (−) TEVp. Blotting was performed using antibodies against HA and α-tubulin. Arrows indicate the 35-kDa E-cad cleavage product. (E) Western blot of lysates from MDCK cells stably expressing Cle-cadHA, grown on Transwell filters and incubated for 3 h with (+) or without (−) TEVp. Blotting was performed using antibodies against HA, E-cadEC, E-cadCD and α-tubulin.
(F) Immunofluorescence images showing Cle-cadHA (anti-HA), total E-cad (anti-E-cadCD) and actin (phalloidin) in transfected cells that were grown on Transwell filters after TEVp treatment. Scale bars: 5 µm. (G) Quantification of the junctional fluorescence intensity of Cle-cadHA, total E-cad and actin (as in F). Data show the mean±s.e.m. (*n*=20 cells for each condition).

Finally, we performed a cell-by-cell analysis using immunofluorescence and observed that TEVp-treated Cle-cadHA-expressing cells had a significantly reduced amount of plasma-membrane-associated E-cad when labelled with anti-E-cadCD (Fig. 5F). Crucially, line-scan analysis of Cle-cadHA-expressing cells after TEVp treatment revealed a 74.8±1.6% reduction in Cle-cadHA levels, which correlated with a 55.5±3.1% reduction in total E-cad at the plasma membrane (Fig. 5G). Therefore, *in vivo* TEVp-treatment of Cle-cadHA-expressing cells led to a ~50% reduction of total E-cad within 3 h. This result is in agreement with the reported functional replacement of endogenous E-cad upon expression of exogenous forms (Nieman et al., 1999; Troxell et al., 1999). We also reproduced these findings using stable MDCK cell lines expressing different levels of E-cadHA (supplementary material Fig. S2F), within which the total level of E-cad remains constant.

Cleavage of the E-cad extracellular domain promotes apical cell extrusion

We then tested our hypothesis that, on its own, extracellular cleavage of E-cad at the plasma membrane of one epithelial cell is sufficient to promote cell extrusion. To do so, we diluted Cle-cadHA-expressing cells 1:10 with wild-type MDCK cells. We found that 53.6±2.3% (±s.e.m.) of Cle-cadHA-expressing cells extruded from the epithelial monolayer after addition of TEVp for 3 h, whereas only 12.6±1.5% of control E-cadHA-expressing cells extruded (Fig. 6A–C; supplementary material Fig. S2G). Furthermore, this extrusion required cells to be mixed in a heterologous cell system, as large patches (more than ten cells) of Cle-cadHA cells did not significantly extrude after TEVp addition (supplementary material Fig. S2H). This highlights a requirement for a relative change in E-cad adhesion between cells to drive cell extrusion. We propose that, although most Cle-cadHA is cleaved, dynamic differences in adhesion will not be

generated in large patches of cells, as all the cells will exhibit similar adhesive properties.

To distinguish whether cell extrusion upon Cle-cadHA cleavage results from the production of an adhesion-deficient form of E-cad or from the release of the soluble E-cad extracellular domain, we transiently transfected MDCK cells with a construct consisting of a fusion of the E-cad cytoplasmic domain to the transmembrane and extracellular domains of the interleukin-2 receptor (IL2R–E-cadCDHA, see Fig. 5A) (Gottardi et al., 2001; Schackmann et al., 2011).

As for Cle-cadHA expression, we investigated the extent to which endogenous E-cad is reduced by the expression of IL2R–E-cadCDHA. We showed that stable MDCK cell lines expressing IL2R–E-cadCDHA had a greatly reduced level (55.4±7.7%) of endogenous E-cad (Fig. 6D) and that transient expression (16 h) of IL2R–E-cadCDHA led to a rapid 62.1±2.1% reduction in plasma-membrane-associated E-cad (within 16 h) (Fig. 6E,F). This is in line with findings that dominant-negative mutants of E-cad that lack adhesive properties downregulate the endogenous levels of full-length E-cad (Nieman et al., 1999; Troxell et al., 1999) through endocytosis and subsequent degradation (Chang et al., 2011). Importantly, analysis of single IL2R–E-cadCDHA-transfected cells in the context of untransfected neighbours revealed that 39.1±0.17% extruded compared with 4.5±0.9% of E-cadHA-transfected cells (Fig. 6C,G).

Overall, these experiments show that extracellular cleavage of E-cad alone promotes epithelial cell extrusion and that this is due to the loss of full-length E-cad adhesion, rather than due to shedding of the E-cad extracellular domain. Moreover, epithelial cell extrusion is efficiently stimulated by conditions under which E-cad adhesion is altered rapidly in a heterologous cell system, with cell extrusion detected in the case of Cle-cadHA cleavage by TEVp within 3 h and with IL2R–E-cadCDHA, within 16 h.

This led us to question whether epithelial cell extrusion was driven by relative changes in E-cad adhesion in a heterologous cell system or whether extrusion was stimulated by the surrounding cells sensing inherent differences in adhesive properties between cells. We depleted E-cad for 7 days, achieving a 46.9±6.4% reduction (supplementary material Fig. S3A). Large patches of E-cad-depleted cells were then visible by immunofluorescence (supplementary material Fig. S3B), but these cells did not extrude. To assay whether cell extrusion was stimulated in a heterologous system, E-cad-depleted cells were re-seeded with wild-type MDCK cells and cultured for 16 h. In this context, 9.2±0.6% of E-cad-depleted cells extruded (Fig. 6C; supplementary material Fig. S3C), indistinguishable from control. We therefore conclude that cell extrusion is driven by rapid changes in adhesive properties, rather than by cells sensing inherent differences in adhesion competence.

Cell extrusion driven by E-cad cleavage precedes apoptosis

Apical cell extrusion in a wild-type epithelial monolayer is normally coupled to apoptosis (Andrade and Rosenblatt, 2011; Kuipers et al., 2014; Lubkov and Bar-Sagi, 2014). Accordingly, we observe that 31.6±1.8% (±s.e.m.) of extruded cells expressing IL2R–E-cadCDHA and 56.6±2% of Cle-cadHA-expressing cells after TEVp treatment, display apoptotic profiles (supplementary material Fig. S4A,B). This, however, also demonstrates that a high number of extruded cells are non-apoptotic. Importantly, as apoptotic cells first die and then extrude, this indicates that extracellular cleavage of E-cad leads to the extrusion of cells through a mechanism that is distinct from
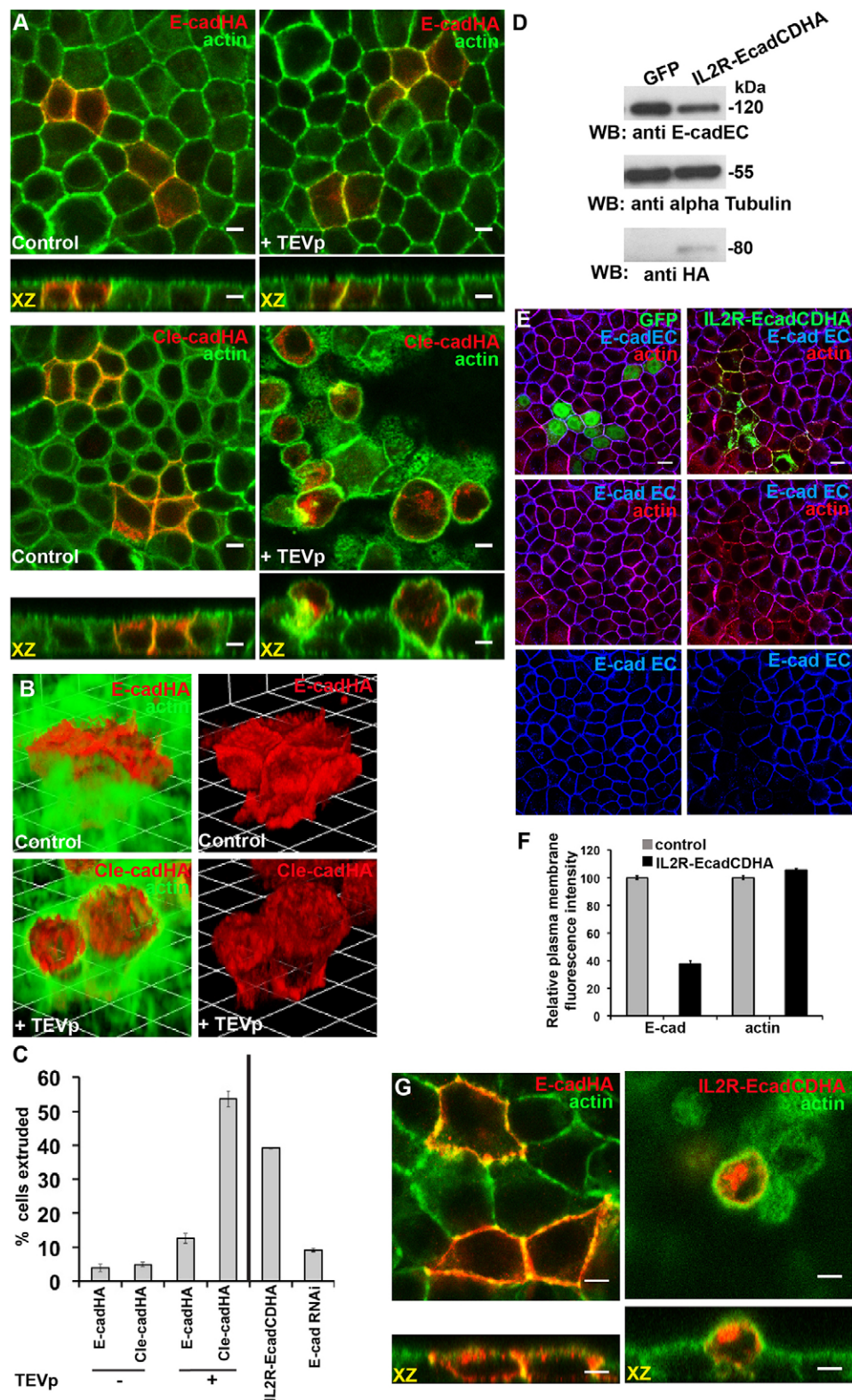
Fig. 6. See next page for legend.

the induction of apoptosis (Rosenblatt et al., 2001; Andrade and Rosenblatt, 2011).

Furthermore, H-RasV12 or CDC42V12 signalling caused extruded cells to proliferate upon the epithelial monolayer (Fig. 1C) (Hogan et al., 2009; Kajita et al., 2010; Leung and

Brugge, 2012). Indeed, we observed that only 2.8±1.4% of extruded cells expressing CDC42V12 displayed apoptotic features (supplementary material Fig. S4A,B). This suggests that apoptosis of extruded cells is inhibited by CDC42 and H-Ras signalling (Hogan et al., 2009; Kajita et al., 2010; Leung and

Fig. 6. Cleavage of the E-cad extracellular domain promotes apical cell extrusion. (A) Immunofluorescence images showing actin (phalloidin, green) and HA (red) to monitor the extrusion of E-cadHA cells (upper panels) or Cle-cadHA cells (lower panels) that were mixed 1:10 with wild-type cells, cultured on Transwell filters and incubated either with TEVp or without it (control). An XZ (orthogonal) view is used to assess cell extrusion. (B) Three-dimensional projections of apical or basal views (using Volocity 3D Image Analysis) of the localisation of E-cadHA or Cle-cadHA (anti-HA, red) and actin (phalloidin, green) in cells expressing E-cadHA or Cle-cadHA and surrounded by wild-type MDCK cells. (C) Quantification of the extrusion of MDCK cells transfected with E-cadHA without TEVp ($n=125$ cells), Cle-cadHA without TEVp ($n=119$ cells), E-cadHA with TEVp ($n=147$ cells), Cle-cadHA with TEVp ($n=99$ cells) or IL2R–E-cadCDHA ($n=110$ cells) and of cells depleted of E-cad by siRNA ($n=66$ cells). Data show the mean±s.e.m. ($n=3$). (D) Western blot (WB) of lysates from MDCK cells stably expressing GFP or IL2R–E-cadCDHA. Blotting was performed using antibodies against HA, E-cadEC and α-tubulin. (E) Immunofluorescence images showing GFP or IL2R–E-cadCDHA (anti-HA), along with endogenous E-cad (anti-E-cadEC) and actin (phalloidin) in cells transiently transfected with GFP or IL2R–E-cadCDHA. (F) Quantification of the plasma-membrane-associated fluorescence intensity of endogenous E-cad and actin of cells transiently transfected with GFP or IL2R–E-cadCDHA (as in Fig. 6E). Data show the mean±s.e.m. ($n=20$ cells for each condition). (G) (Immuno)-fluorescence images showing actin (phalloidin, green) and HA (red) in cells transiently transfected with E-cadHA or IL2R–E-cadCDHA. Scale bars: 5 µm.

Brugge, 2012), in line with the known mechanisms of apoptotic suppression in tumorigenesis (Hanahan and Weinberg, 2011).

DISCUSSION
How does E-cad cleavage mechanistically facilitate extrusion?

E-cad has been shown to be required for cell extrusion (see Introduction). Here, we show that a single cell can be extruded from epithelial monolayers, elicited solely by extracellular cleavage of E-cad. This cleavage generates two fragments that might directly drive epithelial extrusion. Our data indicate that cell extrusion can occur independently of the generation of soluble E-cad fragments, as it can be driven by IL2R–E-cadCDHA expression (Fig. 5F,G). Extrusion also seems to be independent of the membrane-bound cleaved E-cad fragment, as this fragment is barely detectable within the timeframe of extrusion mediated by TEVp and Cle-cad (supplementary material Fig. S2B,C). However, we cannot completely rule out the possibility that this fragment elicits a response within the extruding cell through, for instance, aberrant recruitment of catenins or downstream signalling.

We favour a model in which cell extrusion is governed by rapid changes in adhesive properties, for two reasons. First, TEVp-treated Cle-cadHA-expressing cells and IL2R–E-cadCDHA-expressing cells extrude within relatively short treatment times, during which the full-length E-cad level is reduced. Second, E-cad-depleted cells do not extrude when re-seeded with wild-type MDCKs, suggesting that apical cell extrusion is not simply driven by cells exhibiting differences in adhesive capacity (Fig. 6C; supplementary material Fig. S4). We propose that wild-type cells surrounding either CDC42V12-expressing cells or TEVp-treated Cle-cadHA-expressing cells sense a relative change in adhesion due to E-cad cleavage and respond in a way that drives apical extrusion. In this model, E-cad cleavage quickly renders a cell unable to efficiently adhere to its wild-type neighbours. In response to cleavage of E-cad, the surrounding epithelial cells search for a wild-type partner with cognate E-cad-mediated adhesive and mechanical properties, to restore junctional tension and epithelial integrity. In doing so, the surrounding wild-type cells extend their plasma membranes underneath the extruding

cell (Fig. 1A,D,D′; Fig. 4B; Fig. 6A–C) to form a new adherens junction, which, upon maturation, provides the necessary force for extrusion (Fig. 7). This is supported by the appearance of strong E-cad punctae underneath the extruding cell (Fig. 2B′,C′, double arrows) that presumably corresponds to a new junction being formed. This is distinct from E-cad-based cell sorting, whereby inherent differences in the adhesive competence of different cell populations drive epithelial organisation (Steinberg, 1962).

Our proposal is in line with a model put forward for apoptotic extrusion, now shown to be dependent upon E-cad levels (Lubkov and Bar-Sagi, 2014). In this very recent paper, E-cad was shown to be required for the coordinated elongation of the cells neighbouring an apoptotic cell, after its extrusion, in order to seal the gap and maintain an efficient barrier function. Whether E-cad cleavage has a role in apoptotic extrusion, presumably in triggering the initial extrusion event, has not been investigated.

The contribution of junctional tension to extrusion

Epithelial cell junctions are under significant mechanical tension, of which the cadherin complex is a mechanotransductor (le Duc et al., 2010; Smutny and Yap, 2010; Gomez et al., 2011; Leckband et al., 2011; Budnar and Yap, 2013). It is therefore likely that E-cad cleavage also results in a loss of tension between an extruding cell and its neighbours, which might contribute to extrusion.

Indeed, recent studies have revealed that E-cad and its associated contractile actomyosin cortex is present along the whole apical-lateral interface between epithelial cells, not just at the zonula adherens. The tension generated by the actomyosin network is not uniform, with higher tension exhibited at the zonula adherens (Wu et al., 2014). Importantly, disruption of this tension gradient occurs upon H-Ras transformation, which drives epithelial extrusion. This process involves, and can be stimulated by, a redistribution of N-WASP (officially known as WASL) from the zonula adherens to more lateral regions along the apical-lateral axis. In agreement, as we observe both E-cad and Cle-cad along the entire length of the lateral plasma membrane connecting MDCK cells (supplementary material Fig. S2A; Fig. 7), E-cad cleavage is likely to affect tension along this whole interface. Whether E-cad cleavage causes a shift in N-WASP localisation remains to be investigated.

Are extruding cells passive or active participants?

An interesting question remains as to whether the extruding cell is passive in the extrusion (i.e. only relying on E-cad cleavage at its plasma membrane) or active (i.e. also relying on other cell biological processes, such as the rearrangement of the cortical cytoskeleton and endocytosis). As shown above, both CDC42V12-transfected cells and TEVp-treated Cle-cadHA cells are significantly driven to extrude. However, CDC42V12 cells undergo extrusion more efficiently (90% versus 50%, Fig. 1; Fig. 6A–C). This might be explained by the fact that E-cad cleavage is more efficient in CDC42V12 cells than TEVp-treated Cle-cad cells. Even though our evidence suggests that Cle-cad truncation upon TEVp addition is efficient (Fig. 5D), Cle-cadHA represents only ~50% of the total E-cad pool in our cell line, whereas 100% of the plasma membrane E-cad pool is available for cleavage in CDC42V12-expressing cells. Thus, our data are consistent with a model according to which extrusion efficiency is a measure of the extent of E-cad cleavage.
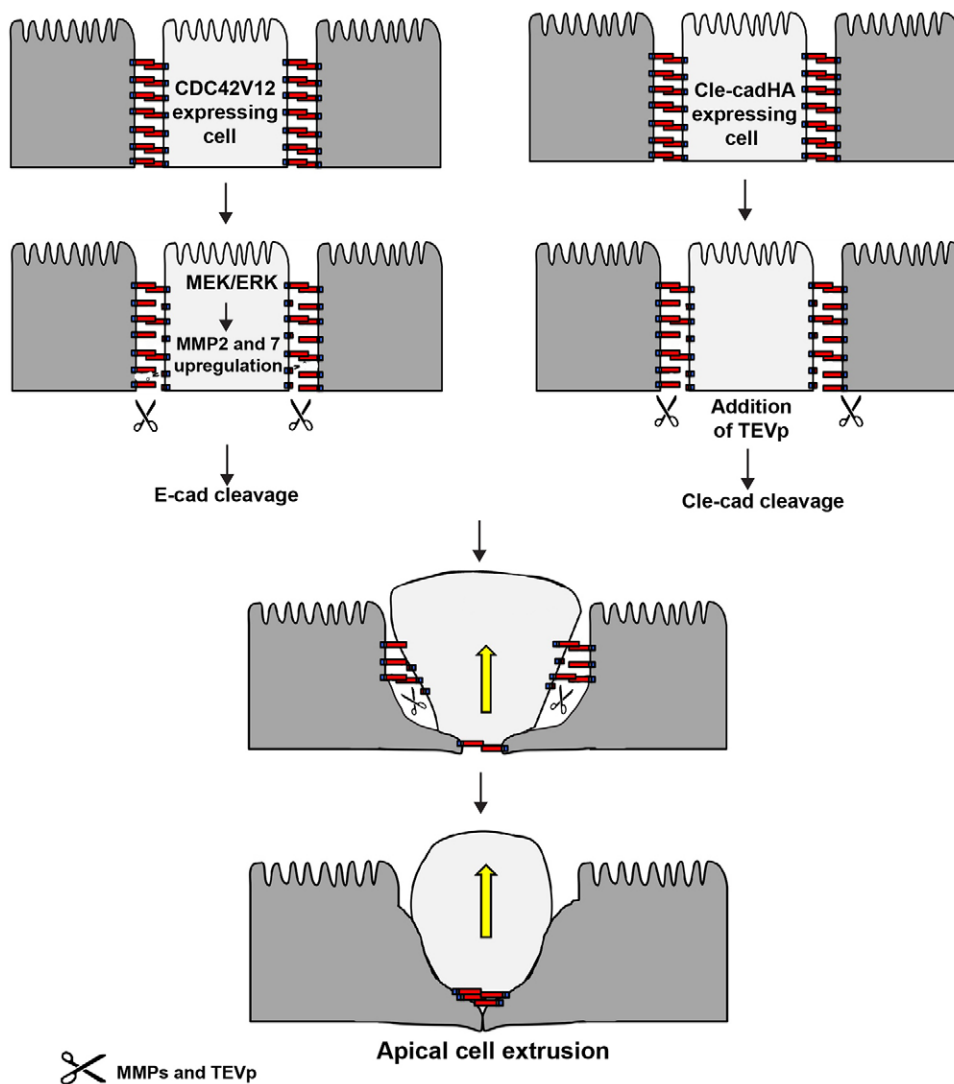
Fig. 7. A model for E-cad-based apical cell extrusion. Cell–cell adhesion can be acutely altered through extracellular cleavage of a pool of E-cad in one cell that is surrounded by wild-type neighbours, giving rise to dynamic changes in adhesion between the cells. Surrounding cells search for neighbours with cognate adhesive properties underneath the adhesion-compromised cell and form a new cell–cell junction, which, upon maturation, is sufficient to drive extrusion of the adhesion-compromised cell. Unless it occurs in the presence of anti-apoptotic oncogenic signalling, extrusion is coupled to apoptosis.

However, other contributory cell biological processes are stimulated within CDC42V12-expressing cells that are not elicited by E-cad cleavage alone, such as actin polymerisation and endocytosis (Georgiou et al., 2008; Leibfried et al., 2008; Shen et al., 2008). A difference in the remodelling of the cortical actin cytoskeleton within CDC42V12-expressing extruding cells is nevertheless unlikely to be responsible for this difference, as dominant-negative Rac1 and RhoA failed to inhibit extrusion (supplementary material Fig. S1B,C). The contribution of the actomyosin network is more likely to be crucial in the surrounding epithelia, which is suggested by previous studies with actomyosin inhibitors (Hogan et al., 2009; Eisenhoffer et al., 2012). Whether a change in endocytosis is observed in CDC42V12-expressing cells has not been investigated. Furthermore, other processes causative to extrusion, such as sphingosine-1-phosphate (S1P) production, could make CDC42V12-driven apical extrusion more efficient than extrusion elicited by Cle-cad and TEVp (Gu et al., 2011). Furthermore, the relative requirements for MEK–ERK signalling

in TEVp-treated Cle-cadHA-expressing extruding cells and CDC42V12-expressing extruding cells have not been studied. An interesting avenue to pursue would be to test whether E-cad cleavage in one cell leads to the activation of the MEK–ERK pathway within surrounding cells. Overall, we favour a model according to which extruding cells signal their own extrusion, either by MMP upregulation (see below), thus cleaving their plasma membrane E-cad, and/or other means, such as S1P production, but also require the concerted actions of neighbouring cells to efficiently extrude.

How are extrusion and E-cad extracellular cleavage mediated in oncogenic contexts?

Many metalloproteinases are known to cleave E-cad (Marambaud et al., 2002; Maretzky et al., 2005). However, to date, the direct cleavage of E-cad during extrusion is undocumented. Here, we show that cells with active CDC42 or H-Ras signalling exhibit increased E-cad cleavage (Fig. 3A,B; supplementary material Fig. S2A). We demonstrate that E-cad cleavage and cell extrusion

in CDC42V12-expressing cells is MMP sensitive, in a similar manner to ERBB2-driven extrusion (Fig. 4). As E-cadHA^{MMP-M} partially inhibits extrusion, we argue that the cleavage of E-cad upon CDC42V12 expression is not simply a correlative marker of cell extrusion, but has a contributory role. Supporting this, truncation of Cle-cadHA by TEVp leads to efficient cell extrusion, demonstrating that E-cad cleavage is sufficient to drive apical cell extrusion (Fig. 6). We cannot, however, exclude the possibility that other proteins might be subject to MMP activity in CDC42V12-transfected cells, such those proteins involved in extracellular matrix attachment and cell–cell adhesion. This could also be another reason for the increased efficiency of CDC42V12-driven extrusion.

Inhibition of MEK–ERK signalling downstream of active Src, H-Ras or CDC42 is sufficient to block apical extrusion (Fig. 1B,D; Fig. 3C) (Hogan et al., 2009; Kajita et al., 2010;). Accordingly, using a candidate-based RT-qPCR screen, we show that CDC42V12 expression leads to the upregulation of MMP2 and MMP7 (Fig. 4D), in a U0126-dependent manner (Fig. 4E). Whether these proteases are causative of CDC42V12-mediated extrusion or can elicit apical cell extrusion alone is the focus of future study. Of note, although we did not test the requirement for the JNK pathway downstream of MEK1 activation, our data are similar to results in *Drosophila*, whereby activated CDC42 results in loss of polarity (Atwood et al., 2007; Joberty et al., 2000), in turn leading to JNK activation (Igaki et al., 2006), itself driving the transcriptional upregulation of MMPs (Uhlirova and Bohmann, 2006; Han et al., 2001). However, to our knowledge, no direct evidence supports MEK–ERK upregulation by CDC42 under physiological conditions. It is possible that this requires strong CDC42 activation, for instance, during oncogenic transformation.

Links between E-cad cleavage and tumorigenesis
Our data are in line with the direct correlation between loss of E-cad adhesion and tumorigenesis (Riethmacher et al., 1995; Gottardi et al., 2001). Mutations in E-cad lead to altered cell morphology, reduced adhesion and human lobular carcinoma (Berx et al., 1995; Handschuh et al., 1999; Cavallaro and Christofori, 2004), and a decreased level of E-cad is a marker of EMT. Importantly, E-cad levels are reduced in some experimental models of cancer but in the absence of mutations or changes in the transcription of E-cad or its associated catenins (Thiery, 2003). This suggests that post-translational mechanisms can give rise to E-cad loss, likely by cleavage as illustrated by the increased level of soluble E-cad extracellular domain in the serum of patients with different cancers (Katayama et al., 1994; Griffiths et al., 1996; Cioffi et al., 1999; Protheroe et al., 1999; Charalabopoulos et al., 2006; Craig and Brady-Kalnay, 2011). This cleavage could be mediated by the many metalloproteinases that have been demonstrated to cleave E-cad (Marambaud et al., 2002; Maretzky et al., 2005; Zheng et al., 2009; Craig and Brady-Kalnay, 2011). For these reasons, a more comprehensive analysis of the proteases that are upregulated during apical cell extrusion might aid our understanding of the events that drive tumorigenesis.

MATERIALS AND METHODS
Chemicals and antibodies
The chemicals used were phalloidin (Invitrogen), MG132 (10 μM, Merck), bafilomycin A (100 nM, Sigma), GM6001 (50 μM, Enzo Life Sciences), U0126 (10 μM, Sigma) and batimastat (10 μM, Sigma). The antibodies used were mouse monoclonal anti-HA (1:1000, clone 16.B12,

Covance), mouse anti-E-cadCD (1:2000, BD Biosciences), mouse anti-E-cadEC (1:100, RR1, DSHB), mouse monoclonal anti-α-tubulin (1:5000, Sigma), mouse monoclonal anti-Myc (9E10, 1:1000, Sigma), rabbit anti-HA (1:500, clone C29F4, Cell Signaling Technology), fluorescently conjugated secondary antibodies (Invitrogen), horseradish peroxidase (HRP)-conjugated secondary antibodies (GE Healthcare), mouse anti-His×6 (1:1000; 631216, Clontech) and mouse anti-FLAG epitope DYKDDDK (Clone FG4R; Thermo Scientific).

Cloning
The Myc-CDC42 wild-type, N17 and V12 constructs were gifts from Hans Bos (University Medical Center, Utrecht, The Netherlands). Constructs expressing FLAG-tagged Rac1 N17 and RhoA N19 were kind gifts from Anne Ridley (King's College London, UK). Constructs expressing MEK1–6×His and MEK1DD–6×His were kind gifts from Manuela Baccharini (Max F. Perutz Laboratories, Vienna, Austria).

For E-cad shRNA, a plasmid expressing GFP and E-cad-specific shRNA (5′-GATCCCCGTCTAACAGGGACAAAGAATTCAAGAGA-TTCTTTGTCCCTGTTAGACTTTTTGGAAA-3′) was a gift from Johan de Rooij (Hubrecht Institute, Utrecht, The Netherlands). For E-cadHA, the canine coding sequence encoded by the E-cadherin-GFP construct was PCR amplified using the forward primer 5′-GGGAATTCATGGGC-CCTCGGTACGGCGGC-3′ and the reverse primer 5′-CCGCGG-CCGCTCAAGCGTAATCTGGAACATCGTATGGGTAGTCGTCCTC-GCCACCTCCATA-3′, introducing an HA tag. This product was digested with *Eco*RI and *Not*I and inserted within pEGFP-N1 between these sites.

For GFP-tagged CDC42V12, the CDC42 coding region of the Myc-CDC42 wild-type construct was amplified with the forward primer 5′-GGCCCGGGCATGCAGACAATTAAGTGTGTTGTTGTGG-3′ and the reverse primer 5′-CCTCTAGATTAGAATATACAGCACTTCC-TTTTGGG-3′, digested with *Xma*I and *Xba*I and inserted within these sites in pEGFP-C1. For GFP–H-RasV12, using a construct expressing H-RasV12 (a gift from Hans Bos), the coding sequence was amplified using the forward primer 5′-GGCTCGAGCGATGACGGAATATAAGCTGG-3′ and the reverse primer 5′-CCGGATCCTCAGGAGAGCACACA-CTTGC-3′, digested with *Xho*I and *Bam*HI and inserted within these sites in pEGFP-C1.

For generating Cle-cadHA, we used E-cadHA as a template for two overlapping PCRs using the primer combinations: (1) forward, 5′-GGGAATTCATGGGCCCTCGGTACGGCGGC-3′; reverse, 5′-GCC CTGGAAATACAAGTTTTCCCTCTTGCAGCTGTTGACGACACC-3′ and (2) forward, 5′-GAAAACTTGTATTTCCAGGGCACGGCGCC-TTACGCCGAAGCAGG-3′; reverse, 5′-CCGCGGCCGCTCAAGCG-TAATCTG-3′. The TEVp recognition sequence was introduced between the transmembrane domain and EC5 of canine E-cadherin by overlapping PCR using the two above products as a template with the forward primer 5′-GGGAATTCATGGGCCCTCGGTACGGCGGC-3′ and the reverse primer 5′-CCGCGGCCGCTCAAGCGTAATCT-GGAACATCGTATGGGTAGTCGTCCTCGCCACCTCCATA-3′. This product was digested with *Eco*RI and *Not*I and was inserted within pEGFP-N1 between these sites.

For IL2R fusion with the canine E-cadherin cytoplasmic domain (IL2R–E-cadCDHA), two overlapping PCRs were performed with the primer combinations: (1) forward, 5′-GGGAATTCATGCATCTAG-CTTGGCGGCTGG-3′; reverse, 5′-CTTTGACCACCCTTCTCCTCC-GAAGCTTCCAGGTGAGCCCACT-3′, using an IL2R-E-cad (human) fusion construct as template (a gift from Patrick Derksen, University Medical Center, Utrecht, The Netherlands), and (2) forward, 5′-CGGAGGAGAAGGGTGGTCAAAG-3′; reverse, 5′-CCGCGGCC-GCTCAAGCGTAATCTG-3′, using E-cadHA as a template. The production of the canine E-cadherin cytoplasmic domain fused to IL2R was achieved by overlapping PCR, using the two above products as a template with the forward primer 5′-GGGAATTCATGCATCT-AGCTTGGCGGCTGG-3′ and the reverse primer 5′-CCGCGGCCGC-TCAAGCGTAATCTG-3′. The product was digested with *Eco*RI and *Not*I and inserted within these sites in pEGFP-N1.

For production of E-cadHA^{MMP}, alanine substitution of Pro702 and Tyr703 was achieved by overlapping PCR. Using E-cadHA as a template,

we performed two overlapping PCRs using the primer combinations: (1) forward, 5′-GGGAATTCATGGGCCCTCGGTACGGCGGC-3′; reverse, 5′-CCTGCAAGCCTGCTTCGGCGGCAGCCGCCGTCCTCTTGCAG-CTGT-3′ and (2) forward, 5′-ACAGCTGCAAGAGGACGGCGG-CTGCCGCCGAAGCAGGCTTGCAGG-3′; reverse, 5′-CCGCGGC-CGCTCAAGCGTAATCTG-3′. This product was digested with *EcoR*I and *Not*I and inserted within pEGFP-N1 between these sites. All plasmids were fully sequenced (Macrogen Europe).

Mammalian cell culture, transfection and treatments

MDCKII cells were grown as described previously (Grieve et al., 2011). To generate MDCK lines stably expressing E-cadHA and Cle-cadHA, cells were transfected with 2 µg of cDNA carrying neomycin resistance for 6 h with 5 µl of Lipofectamine-2000 (Invitrogen). After 6 h, cells were washed with PBS and returned to regular medium for 2 days. Cells were selected in regular medium containing 500 µg/ml G418. G418-resistant E-cadHA and Cle-cadHA colonies were established, tested for similar HA expression levels and expanded. For transient (co)-transfections, cells grown for 3–4 days were transfected at ~80–90% confluence with 2 µg of cDNA for each construct for 2–4 h, yielding ~10% transfection efficiency as above.

For Cle-cad and TEVp experiments, $\geq 2 \times 10^5$ cells/cm^2 were seeded onto Transwell® inserts (12-well, polyester membranes, 0.4-µm pore) for 36 h. Purified TEVp at ~200 µg/ml (a kind gift from Madelon Maurice, University Medical Center, Utrecht, The Netherlands) in TEVp buffer [50 mM Tris-HCl, 500 µM EDTA and 1 mM dithiothreitol (DTT) in DMEM containing 1% fetal calf serum] was added to basal compartments.

For E-cad depletion, cells were transfected with GFP and E-cad-specific shRNA-expressing plasmid and grown for 7 days. Cells were trypsinised, replated with wild-type MDCK cells and grown for 16 h.

Immunoprecipitation

Lysates and supernatants were prepared in 1 ml of ice-cold lysis buffer (50 mM Tris-HCl, 150 mM NaCl, 2% Triton X-100, 1 mM MgCl$_2$, 1 mM EDTA and 0.5 mM DTT) in the presence of protease inhibitor cocktail (Roche), as described previously (Grieve et al., 2011). Supernatants were added to Protein-A–agarose beads (Pierce) that had been pre-coated overnight with the indicated antibodies at 4°C for 2 h. Beads were washed and prepared for SDS-PAGE or TEVp treatment. For *in vitro* incubations with 30 µg of TEVp, 30 µl of beads bound to Cle-cadHA immunoprecipitated from transiently transfected cells were washed and incubated at 37°C for 3 h in TEVp buffer. Sample loading was one quarter of the bead volume.

Plasma membrane biotinylation and streptavidin pull downs

All buffers and steps were on ice. Cells were washed six times with PBS. After incubation with 1 mg/ml EZ-Link Sulfo-NHS-LC-Biotin (Fisher Scientific), cells were washed three times followed by a 10 min quench with 100 mM glycine in PBS. Cells were lysed and prepared as stated for immunoprecipitations, and added to pre-washed high-capacity streptavidin–agarose beads (Fisher Scientific) for 1 h at 4°C. After five washes in lysis buffer, the beads were prepared for SDS-PAGE.

SDS-PAGE and western blotting

Samples were run and transferred as described previously (Grieve et al., 2011). Membranes were subjected to overnight primary antibody incubations at 4°C and were subsequently incubated with HRP-conjugated secondary antibodies (GE Healthcare). Band visualisation was achieved with Enhanced Chemiluminescence (Amersham Biosciences) using Kodak X-ray film.

Immunofluorescence microscopy

Cells were fixed with 4% paraformaldehyde in PBS for 20 min at room temperature, quenched with 50 µM NH$_4$Cl, permeabilised by treatment with 0.2% Triton X-100 in PBS and blocked in PBS supplemented with 1% fish-skin gelatin before incubation with primary and secondary antibodies. ProLong® Gold Antifade Reagent with DAPI was used for confocal imaging (Leica SPE) at room temperature (63× NA1.4 objective) using LCS software (Leica).

RNA Isolation and RT-qPCR

Total RNA was extracted using the RNeasy mini kit (Qiagen). Isolated RNA was treated with RNase-free DNase I (Sigma). The GoScript^{TM} Reverse Transcription System (Promega) was used to generate either poly(A)-positive mRNA with oligo-dT primers or mRNA with random hexamers. Reverse transcription and real-time RT-PCR were carried out as described previously (Giuliani et al., 2014). GAPDH mRNA transcripts were used as a control. The sequences of primers used are listed in supplementary material Table S1. Relative quantification was achieved as described previously (Giuliani et al., 2014).

Quantification

Cell extrusion

Cells were selected by the presence of similar levels of GFP or HA immunolabelling between conditions. Cell extrusion was defined by the following features: rounding up of the extruding cell, at least half the cell diameter being above the apical membranes of the surrounding untransfected cells and the appearance of a basal actin accumulation beneath the extruding cell. Basal actin is rarely observed underneath epithelial cells, thus is indicative that surrounding cells have protruded membrane underneath the extruding cell. Error bars represent s.e.m. ($n \geq 3$).

Immunofluorescence

Line-scan analysis of Cle-cadHA, total E-cad and actin with or without TEVp treatment and of IL2R–E-cadCDHA-transfected cells was performed upon individual confocal sections. 1-µm-wide lines were drawn at lateral membrane positions in line with the cell nucleus. For the analysis of E-cadEC and actin at the plasma membrane of GFP- and GFP–CDC42V12-transfected cells, 1-µm-wide lines were drawn at three positions (designated in the figure) along the lateral membrane and analysed using the Plot Profile tool in ImageJ. Plasma membrane position was determined by the peak grey value for actin, and the corresponding E-cad grey value is displayed with respect to the actin peak position. Error bars represent s.e.m. ($n=3$).

Western blots

Band intensities were determined using the Analyse Gels tool in ImageJ and were normalised to loading controls and measurements taken for control treatments. Error bars represent s.e.m. ($n \geq 3$).

Supplementary material

Supplementary material available online at
http://jcs.biologists.org/lookup/suppl/doi:10.1242/jcs.147926/-/DC1

References

Andrade, D. and Rosenblatt, J. (2011). Apoptotic regulation of epithelial cellular extrusion. *Apoptosis* **16**, 491-501.

Atwood, S. X., Chabu, C., Penkert, R. R., Doe, C. Q. and Prehoda, K. E. (2007). Cdc42 acts downstream of Bazooka to regulate neuroblast polarity through Par-6 aPKC. *J. Cell Sci.* **120**, 3200-3206.

Baum, B. and Georgiou, M. (2011). Dynamics of adherens junctions in epithelial establishment, maintenance, and remodeling. *J. Cell Biol.* **192**, 907-917.

Berx, G., Cleton-Jansen, A. M., Nollet, F., de Leeuw, W. J., van de Vijver, M., Cornelisse, C. and van Roy, F. (1995). E-cadherin is a tumour/invasion suppressor gene mutated in human lobular breast cancers. *EMBO J.* **14**, 6107-6115.

Budnar, S. and Yap, A. S. (2013). A mechanobiological perspective on cadherins and the actin-myosin cytoskeleton. *F1000Prime Rep.* **5**, 35.

Capaldo, C. T. and Macara, I. G. (2007). Depletion of E-cadherin disrupts establishment but not maintenance of cell junctions in Madin-Darby canine kidney epithelial cells. *Mol. Biol. Cell* **18**, 189-200.

Cavallaro, U. and Christofori, G. (2004). Cell adhesion and signalling by cadherins and Ig-CAMs in cancer. *Nat. Rev. Cancer* **4**, 118-132.

Chang, L. H., Chen, P., Lien, M. T., Ho, Y. H., Lin, C. M., Pan, Y. T., Wei, S. Y. and Hsu, J. C. (2011). Differential adhesion and actomyosin cable collaborate to drive Echinoid-mediated cell sorting. *Development* **138**, 3803-3812.

Charalabopoulos, K., Gogali, A., Dalavaga, Y., Daskalopoulos, G., Vassiliou, M., Bablekos, G., Karakosta, A. and Constantopoulos, S. (2006). The clinical significance of soluble E-cadherin in nonsmall cell lung cancer. *Exp. Oncol.* **28**, 83-85.

Chitaev, N. A. and Troyanovsky, S. M. (1998). Adhesive but not lateral E-cadherin complexes require calcium and catenins for their formation. *J. Cell Biol.* **142**, 837-846.

Cioffi, M., Gazzerro, P., Di Finizio, B., Vietri, M. T., Di Macchia, C., Puca, G. A. and Molinari, A. M. (1999). Serum-soluble E-cadherin fragments in lung cancer. *Tumori* **85**, 32-34.

Coso, O. A., Chiariello, M., Yu, J. C., Teramoto, H., Crespo, P., Xu, N., Miki, T. and Gutkind, J. S. (1995). The small GTP-binding proteins Rac1 and Cdc42 regulate the activity of the JNK/SAPK signaling pathway. *Cell* **81**, 1137-1146.

Craig, S. E. and Brady-Kalnay, S. M. (2011). Cancer cells cut homophilic cell adhesion molecules and run. *Cancer Res.* **71**, 303-309.

Denning, D. P., Hatch, V. and Horvitz, H. R. (2012). Programmed elimination of cells by caspase-independent cell extrusion in C. elegans. *Nature* **488**, 226-230.

Desai, R., Sarpal, R., Ishiyama, N., Pellikka, M., Ikura, M. and Tepass, U. (2013). Monomeric α-catenin links cadherin to the actin cytoskeleton. *Nat. Cell Biol.* **15**, 261-273.

Eisenhoffer, G. T. and Rosenblatt, J. (2013). Bringing balance by force: live cell extrusion controls epithelial cell numbers. *Trends Cell Biol.* **23**, 185-192.

Eisenhoffer, G. T., Loftus, P. D., Yoshigi, M., Otsuna, H., Chien, C. B., Morcos, P. A. and Rosenblatt, J. (2012). Crowding induces live cell extrusion to maintain homeostatic cell numbers in epithelia. *Nature* **484**, 546-549.

Fanger, G. R., Johnson, N. L. and Johnson, G. L. (1997). MEK kinases are regulated by EGF and selectively interact with Rac/Cdc42. *EMBO J.* **16**, 4961-4972.

Fujita, Y., Krause, G., Scheffner, M., Zechner, D., Leddy, H. E., Behrens, J., Sommer, T. and Birchmeier, W. (2002). Hakai, a c-Cbl-like protein, ubiquitinates and induces endocytosis of the E-cadherin complex. *Nat. Cell Biol.* **4**, 222-231.

Georgiou, M., Marinari, E., Burden, J. and Baum, B. (2008). Cdc42, Par6, and aPKC regulate Arp2/3-mediated endocytosis to control local adherens junction stability. *Curr. Biol.* **18**, 1631-1638.

Giuliani, G., Giuliani, F., Volk, T. and Rabouille, C. (2014). The Drosophila RNA-binding protein HOW controls the stability of dgrasp mRNA in the follicular epithelium. *Nucleic Acids Res.* **42**, 1970-1986.

Gomez, G. A., McLachlan, R. W. and Yap, A. S. (2011). Productive tension: force-sensing and homeostasis of cell-cell junctions. *Trends Cell Biol.* **21**, 499-505.

Gottardi, C. J., Wong, E. and Gumbiner, B. M. (2001). E-cadherin suppresses cellular transformation by inhibiting beta-catenin signaling in an adhesion-independent manner. *J. Cell Biol.* **153**, 1049-1060.

Grieve, A. G., Daniels, R. D., Sanchez-Heras, E., Hayes, M. J., Moss, S. E., Matter, K., Lowe, M. and Levine, T. P. (2011). Lowe Syndrome protein OCRL1 supports maturation of polarized epithelial cells. *PLoS ONE* **6**, e24044.

Griffiths, T. R., Brotherick, I., Bishop, R. I., White, M. D., McKenna, D. M., Horne, C. H., Shenton, B. K., Neal, D. E. and Mellon, J. K. (1996). Cell adhesion molecules in bladder cancer: soluble serum E-cadherin correlates with predictors of recurrence. *Br. J. Cancer* **74**, 579-584.

Gu, Y., Forostyan, T., Sabbadini, R. and Rosenblatt, J. (2011). Epithelial cell extrusion requires the sphingosine-1-phosphate receptor 2 pathway. *J. Cell Biol.* **193**, 667-676.

Gumbiner, B. M. (2000). Regulation of cadherin adhesive activity. *J. Cell Biol.* **148**, 399-404.

Han, Z., Boyle, D. L., Chang, L., Bennett, B., Karin, M., Yang, L., Manning, A. M. and Firestein, G. S. (2001). c-Jun N-terminal kinase is required for

metalloproteinase expression and joint destruction in inflammatory arthritis. *J. Clin. Invest.* **108**, 73-81.

Hanahan, D. and Weinberg, R. A. (2011). Hallmarks of cancer: the next generation. *Cell* **144**, 646-674.

Handschuh, G., Candidus, S., Luber, B., Reich, U., Schott, C., Oswald, S., Becke, H., Hutzler, P., Birchmeier, W., Höfler, H. et al. (1999). Tumour-associated E-cadherin mutations alter cellular morphology, decrease cellular adhesion and increase cellular motility. *Oncogene* **18**, 4301-4312.

Harris, K. P. and Tepass, U. (2010). Cdc42 and vesicle trafficking in polarized cells. *Traffic* **11**, 1272-1279.

Hartsock, A. and Nelson, W. J. (2012). Competitive regulation of E-cadherin juxtamembrane domain degradation by p120-catenin binding and Hakai-mediated ubiquitination. *PLoS ONE* **7**, e37476.

Hogan, C., Dupré-Crochet, S., Norman, M., Kajita, M., Zimmermann, C., Pelling, A. E., Piddini, E., Baena-López, L. A., Vincent, J. P., Itoh, Y. et al. (2009). Characterization of the interface between normal and transformed epithelial cells. *Nat. Cell Biol.* **11**, 460-467.

Igaki, T., Pagliarini, R. A. and Xu, T. (2006). Loss of cell polarity drives tumor growth and invasion through JNK activation in Drosophila. *Curr. Biol.* **16**, 1139-1146.

Joberty, G., Petersen, C., Gao, L. and Macara, I. G. (2000). The cell-polarity protein Par6 links Par3 and atypical protein kinase C to Cdc42. *Nat. Cell Biol.* **2**, 531-539.

Kajita, M., Hogan, C., Harris, A. R., Dupre-Crochet, S., Itasaki, N., Kawakami, K., Charras, G., Tada, M. and Fujita, Y. (2010). Interaction with surrounding normal epithelial cells influences signalling pathways and behaviour of Src-transformed cells. *J. Cell Sci.* **123**, 171-180.

Katayama, M., Hirai, S., Kamihagi, K., Nakagawa, K., Yasumoto, M. and Kato, I. (1994). Soluble E-cadherin fragments increased in circulation of cancer patients. *Br. J. Cancer* **69**, 580-585.

Kuipers, D., Mehonic, A., Kajita, M., Peter, L., Fujita, Y., Duke, T., Charras, G. and Gale, J. E. (2014). Epithelial repair is a two-stage process driven first by dying cells and then by their neighbours. *J. Cell Sci.* **127**, 1229-1241.

le Duc, Q., Shi, Q., Blonk, I., Sonnenberg, A., Wang, N., Leckband, D. and de Rooij, J. (2010). Vinculin potentiates E-cadherin mechanosensing and is recruited to actin-anchored sites within adherens junctions in a myosin II-dependent manner. *J. Cell Biol.* **189**, 1107-1115.

Leckband, D. E., le Duc, Q., Wang, N. and de Rooij, J. (2011). Mechanotransduction at cadherin-mediated adhesions. *Curr. Opin. Cell Biol.* **23**, 523-530.

Leibfried, A., Fricke, R., Morgan, M. J., Bogdan, S. and Bellaiche, Y. (2008). Drosophila Cip4 and WASp define a branch of the Cdc42-Par6-aPKC pathway regulating E-cadherin endocytosis. *Curr. Biol.* **18**, 1639-1648.

Leung, C. T. and Brugge, J. S. (2012). Outgrowth of single oncogene-expressing cells from suppressive epithelial environments. *Nature* **482**, 410-413.

Lincoln, D. W., II and Bove, K. (2005). The transcription factor Ets-1 in breast cancer. *Front. Biosci.* **10**, 506-511.

Lubkov, V. and Bar-Sagi, D. (2014). E-cadherin-mediated cell coupling is required for apoptotic cell extrusion. *Curr. Biol.* **24**, 868-874.

Marambaud, P., Shioi, J., Serban, G., Georgakopoulos, A., Sarner, S., Nagy, V., Baki, L., Wen, P., Efthimiopoulos, S., Shao, Z. et al. (2002). A presenilin-1/gamma-secretase cleavage releases the E-cadherin intracellular domain and regulates disassembly of adherens junctions. *EMBO J.* **21**, 1948-1956.

Maretzky, T., Reiss, K., Ludwig, A., Buchholz, J., Scholz, F., Proksch, E., de Strooper, B., Hartmann, D. and Saftig, P. (2005). ADAM10 mediates E-cadherin shedding and regulates epithelial cell-cell adhesion, migration, and beta-catenin translocation. *Proc. Natl. Acad. Sci. USA* **102**, 9182-9187.

Marinari, E., Mehonic, A., Curran, S., Gale, J., Duke, T. and Baum, B. (2012). Live-cell delamination counterbalances epithelial growth to limit tissue overcrowding. *Nature* **484**, 542-545.

Minden, A., Lin, A., Claret, F. X., Abo, A. and Karin, M. (1995). Selective activation of the JNK signaling cascade and c-Jun transcriptional activity by the small GTPases Rac and Cdc42Hs. *Cell* **81**, 1147-1157.

Nieman, M. T., Kim, J. B., Johnson, K. R. and Wheelock, M. J. (1999). Mechanism of extracellular domain-deleted dominant negative cadherins. *J. Cell Sci.* **112**, 1621-1632.

Nowell, P. C. (1976). The clonal evolution of tumor cell populations. *Science* **194**, 23-28.

Patel, S. D., Chen, C. P., Bahna, F., Honig, B. and Shapiro, L. (2003). Cadherin-mediated cell-cell adhesion: sticking together as a family. *Curr. Opin. Struct. Biol.* **13**, 690-698.

Protheroe, A. S., Banks, R. E., Mzimba, M., Porter, W. H., Southgate, J., Singh, P. N., Bosomworth, M., Harnden, P., Smith, P. H., Whelan, P. et al. (1999). Urinary concentrations of the soluble adhesion molecule E-cadherin and total protein in patients with bladder cancer. *Br. J. Cancer* **80**, 273-278.

Riethmacher, D., Brinkmann, V. and Birchmeier, C. (1995). A targeted mutation in the mouse E-cadherin gene results in defective preimplantation development. *Proc. Natl. Acad. Sci. USA* **92**, 855-859.

Rosenblatt, J., Raff, M. C. and Cramer, L. P. (2001). An epithelial cell destined for apoptosis signals its neighbors to extrude it by an actin- and myosin-dependent mechanism. *Curr. Biol.* **11**, 1847-1857.

Schackmann, R. C., van Amersfoort, M., Haarhuis, J. H., Vlug, E. J., Halim, V. A., Roodhart, J. M., Vermaat, J. S., Voest, E. E., van der Groep, P., van Diest, P. J. et al. (2011). Cytosolic p120-catenin regulates growth of metastatic lobular carcinoma through Rock1-mediated anoikis resistance. *J. Clin. Invest.* **121**, 3176-3188.

Shen, Y., Hirsch, D. S., Sasiela, C. A. and Wu, W. J. (2008). Cdc42 regulates E-cadherin ubiquitination and degradation through an epidermal growth factor receptor to Src-mediated pathway. *J. Biol. Chem.* **283**, 5127-5137.

Slattum, G., Gu, Y., Sabbadini, R. and Rosenblatt, J. (2014). Autophagy in oncogenic K-Ras promotes basal extrusion of epithelial cells by degrading S1P. *Curr. Biol.* **24**, 19-28.

Smutny, M. and Yap, A. S. (2010). Neighborly relations: cadherins and mechanotransduction. *J. Cell Biol.* **189**, 1075-1077.

Steinberg, M. S. (1962). On the mechanism of tissue reconstruction by dissociated cells. I. Population kinetics, differential adhesiveness. and the absence of directed migration. *Proc. Natl. Acad. Sci. USA* **48**, 1577-1582.

Tapon, N. and Hall, A. (1997). Rho, Rac and Cdc42 GTPases regulate the organization of the actin cytoskeleton. *Curr. Opin. Cell Biol.* **9**, 86-92.

Thiery, J. P. (2003). Epithelial-mesenchymal transitions in development and pathologies. *Curr. Opin. Cell Biol.* **15**, 740-746.

Troxell, M. L., Chen, Y. T., Cobb, N., Nelson, W. J. and Marrs, J. A. (1999). Cadherin function in junctional complex rearrangement and posttranslational control of cadherin expression. *Am. J. Physiol.* **276**, C404-C418.

Uhlirova, M. and Bohmann, D. (2006). JNK- and Fos-regulated Mmp1 expression cooperates with Ras to induce invasive tumors in *Drosophila*. *EMBO J.* **15**, 5294-5304.

Wu, S. K., Gomez, G. A., Michael, M., Verma, S., Cox, H. L., Lefevre, J. G., Parton, R. G., Hamilton, N. A., Neufeld, Z. and Yap, A. S. (2014). Cortical F-actin stabilization generates apical-lateral patterns of junctional contractility that integrate cells into epithelia. *Nat. Cell Biol.* **16**, 167-178.

Zheng, G., Lyons, J. G., Tan, T. K., Wang, Y., Hsu, T. T., Min, D., Succar, L., Rangan, G. K., Hu, M., Henderson, B. R. et al. (2009). Disruption of E-cadherin by matrix metalloproteinase directly mediates epithelial-mesenchymal transition downstream of transforming growth factor-beta1 in renal tubular epithelial cells. *Am. J. Pathol.* **175**, 580-591.